Available online at www.sciencedirect.com
ScienceDirect
International Journal of Heat and Mass Transfer 51 (2008) 4551–4562
International Journal of HEAT and MASS TRANSFER
www.elsevier.com/locate/ijhmt

Optimization of zeta potential distributions for minimal dispersion in an electroosmotic microchannel

Hwa Sung Woo, Byung Jun Yoon, In Seok Kang *

Department of Chemical Engineering, Pohang University of Science and Technology, San 31, Hyoja Dong, Pohang, South Korea

Received 6 November 2006; received in revised form 18 May 2007
Available online 8 April 2008

Abstract

Optimization of the zeta potential distributions at the walls for minimal dispersion in an electroosmotic microchannel is performed based on the variational approach. In the present problem, the governing equations are the steady flow equations and the unsteady mass transport equation. Based on the calculus of variations and the method of Lagrange multiplier, the Euler–Lagrange equations are derived in the form of coupled partial differential equations. The coupled equations of the state variables and the adjoint variables are solved by the FDM method iteratively. The original and adjoint flow equations are reformulated using the streamfunction-vorticity method to eliminate the pressure and the adjoint pressure in the equations. It is found that the dispersion can be reduced drastically by controlling the zeta potentials at the channel walls in an optimal way. The results of the optimal solutions are expected to provide an insight for the design of zeta potential control systems. The methodology used in this work may find various applications in the area of the micro-total-analysis-system (μTAS).

Keywords: Optimization; Zeta potential; Minimal dispersion; Microchannel; Electroosmotic flow; Variational method; Optimal boundary control

1. Introduction

Multifunctional microchannel systems like lab-on-a-chip devices should request long channel length. A channel about 20 cm in length is required for an electrically driven separation process [1]. Therefore, turns are integrated into microchannel systems for miniaturizing chips. On the other hand, electroosmotic flows (EOFs) have been regarded as an efficient tool for transporting microfluids. Unfortunately, however, the turns of electroosmotic microchannels produce unwanted dispersion induced by variations in the strength of electric field and in the traveling distance (the so-called race track effect). These effects drastically reduce the separation efficiency [1].

There have been many efforts for minimizing the dispersion induced by the turns. Some of them [2–8] are through the modification of channel geometry. Especially, Griffiths and Nilson [7] and Molho et al. [8] studied on the optimal geometrical shape of the turn for minimizing dispersion. On the other hand, there are several methods to control dispersion without changing the geometry or the configuration of turns. One of them is to control zeta potential at the wall. In EOF systems, flow patterns are determined by the zeta potential distributions at the walls and the applied electric field. By experiments, it has been reported that the dispersion can be decreased by controlling the zeta potential values at the walls and that 2D numerical analysis well interprets the experimental results [9,10]. In addition, Qiao and Aluru [11] proposed the optimal control condition of the zeta potential at the inside wall of a turn in nanochannel systems based on numerical results. Woo [12] also investigated the optimal conditions of the zeta potential values at the inside and outside walls of a turn.

In the works of Qiao and Aluru [11] and Woo [12], only very restricted problems for the zeta potential control are considered. They determined the optimal values of the

* Corresponding author. Tel.: +82 54 279 2273; fax: +82 54 279 2699.
E-mail address: iskang@postech.ac.kr (I.S. Kang).

0017-9310/$ - see front matter © 2008 Elsevier Ltd. All rights reserved.
doi:10.1016/j.ijheatmasstransfer.2008.02.008

constant zeta potential at certain parts of the walls. In other words, they considered one or two parameter systems. Consequently, the jump of zeta potential value is allowed. According to Woo [12], it is reported that the step change of the zeta potential value is a possible reason of inducing dispersion. Thus, it is believed that previous efforts for determining optimal conditions of the zeta potential distributions are not sufficient. Therefore, using a systematic approach of optimization, we seek the optimal conditions for the control of zeta potential distributions at inner and outer walls. We define an optimization problem for the control of zeta potential distributions to minimize dispersion and introduce an objective function based on the concentration of the analyte. In order to solve the optimization problem with the equality constraints given by the governing partial differential equations (PDEs) – the steady flow equations and the unsteady transport equation, the variational method is used. Based on the calculus of variations and the method of Lagrange multiplier, we derive an optimality system of equations, the so-called Euler–Lagrange equations in the form of coupled partial differential equations. We solve the system of equations using the finite-difference scheme with iteration and relaxation.

Mathematically, the optimization problem in this work is an optimal boundary control problem for a distributed parameter system described by PDEs. For the studies in that area, the calculus of variations plays the most important role as a general technique for optimization in function spaces [13,14]. It is also in common use for the optimization of flow control [15]. Most of researches for flow control considered only the governing equations of flow (the Navier–Stokes equation and the continuity equation). In steady [16] or unsteady [17–23] flow systems, the researchers solved the optimal flow control problems for minimal stress or vortex and so forth. In a magnetohydrodynamics (MHD) system, the flow field and the magnetic field are coupled. Therefore, the researchers [24–26] investigated the optimization problems with the governing equations coupled by the flow field and the magnetic field. Also, Collis et al. [27] studied on the optimal flow control problem coupled by the flow and the temperature.

In this work, we investigate a new type problem of optimal boundary control problem with the steady flow equations and the unsteady transport equation. The flow field is governed by the steady Stokes equation and the continuity equation. However, the concentration is governed by the unsteady transport equation.

From the results of the optimization problem, we can determine the optimal zeta potential distributions at the walls. The optimal solutions are expected to provide valuable information of the optimal control for minimal dispersion and an insight for the design of zeta potential control systems. Since the optimal flow control problems coupled with the transport equation are important in the micro-total-analysis-systems (μTAS) [28], the methodology proposed in this work may be used as a useful tool to solve such optimal boundary control problems.

2. Problem statement

2.1. Governing equations in an electroosmotic microchannel

We are interested in the control of the zeta potential distributions at the walls for minimization of dispersion in an electroosmotic microchannel. In the present work, we consider a two-dimensional microchannel. Rigorous speaking, the 2D approximation is valid only when the microchannel depth is much large than the width. Nevertheless, the 2D results are still expected to provide an insight also for realistic situations. In addition, the methodology adopted in this work can be easily extended to the more realistic 3D microchannels.

We assume that the microchannel system has a constant width as shown in Fig. 1. W^* and L^* are the channel width and the length of straight a part of channel length. R_i^* and R_o^* are the inside radius and the outside radius. Here, the superscript $*$ denotes the dimensional quantities. Ω_i represents the ith part of the system domain. Ω_1 and Ω_3 are the straight parts and Ω_2 is the curved part. The boundaries are denoted by Γ_i. Γ_1 and Γ_3 are the inlet and the outlet boundaries. Γ_{21}, Γ_{22} and Γ_{23} are the parts of the boundary at the inside wall. Γ_{41}, Γ_{42}, and Γ_{43} are for the outside wall. Vectors $\mathbf{n}$ and $\mathbf{t}$ are the outward normal vector and the tangential vector.

In this work, the physical properties are constant except for the zeta potential distributions. The microchannel walls are impermeable and nonconducting. In a microchannel, the channel dimension is much larger than the Debye length. The Debye layer can be ignored and the charge den-

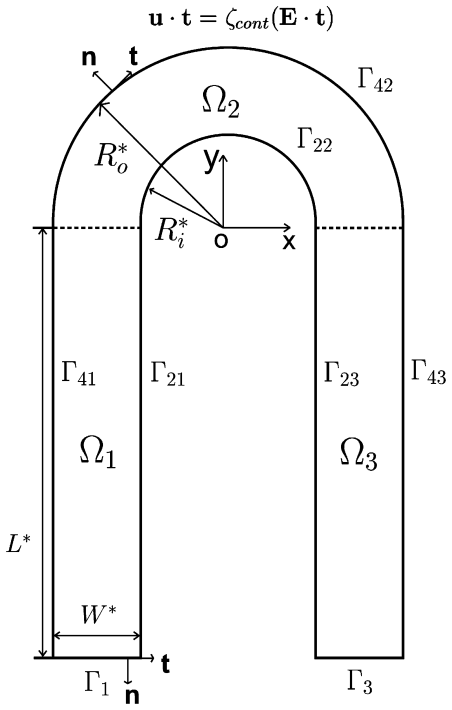

Fig. 1. Schematic of a U-turn microchannel.

sity outside the Debye layer can be assumed to be zero. Therefore, the dimensionless governing equation for the electric potential is the Laplace equation

$$\nabla^2\phi = 0 \tag{1}$$

with the boundary conditions

$$\mathbf{n}\cdot\nabla\phi = 1 \text{ on } \Gamma_1, \quad \phi = 1 \text{ on } \Gamma_3 \tag{2}$$

$$\mathbf{n}\cdot\nabla\phi = 0 \text{ on } \Gamma_{2i} \text{ and } \Gamma_{4i}, \quad i = 1\text{–}3 \tag{3}$$

where the length scale $L_c = W^*$, the electric field scale $E_c = E^*_{\text{inlet}}$ and the electric potential scale $\phi_c = \phi^*_{\text{outlet}}$ are used as the characteristic scales. In the above, the inlet boundary condition is defined by the strength of the electric field and the outlet boundary condition is from the condition of the reference potential.

For the EOF in a microchannel, we can assume that inertial effect is negligible because the fluid velocity is slow and the length scale is also quite small. Therefore, the dimensionless governing equations for the flow field are the continuity equation and the Stokes equation

$$\nabla\cdot\mathbf{u} = 0 \tag{4}$$

$$\nabla^2\mathbf{u} - \nabla p = 0 \tag{5}$$

with the boundary conditions

$$\mathbf{u}\cdot\mathbf{n} = -1, \quad \mathbf{u}\cdot\mathbf{t} = 0 \text{ on } \Gamma_1 \tag{6}$$

$$\mathbf{u}\cdot\mathbf{n} = 0, \quad \mathbf{u}\cdot\mathbf{t} = \zeta_{\text{cont}}(\mathbf{E}\cdot\mathbf{t}) \text{ on } \Gamma_{2i} \text{ and } \Gamma_{4i}, \quad i = 1\text{–}3 \tag{7}$$

$$\mathbf{n}\cdot\nabla(\mathbf{u}\cdot\mathbf{n}) = 0, \quad \mathbf{u}\cdot\mathbf{t} = 0 \text{ on } \Gamma_3 \tag{8}$$

where the zeta potential scale $\zeta_c = |\,\zeta^*_{\text{wall}}\,|$ and the velocity scale $u_c = \epsilon^*\zeta_c E_c/\mu^*$ (Helmholtz–Smoluchowski speed) are used. For convenience, the normalized zeta potential value is defined as $\zeta = -\zeta^*/\zeta_c$. The boundary conditions for the flow field are given by the Dirichlet condition at the inlet and the fully developed condition at the outlet. At the walls, the boundary conditions for the flow field are given by the slip condition based on the Helmholtz–Smoluchowski speed. The zeta potential distributions ζ_{cont} are the control variables.

For the concentration of the analyte, the transport equation is defined as

$$\frac{\partial c}{\partial t} + \mathbf{u}\cdot\nabla c = \frac{1}{Pe}\nabla^2 c \tag{9}$$

with the boundary conditions

$$c = 0 \text{ on } \Gamma_1, \quad \mathbf{n}\cdot\nabla c = 0 \text{ on } \Gamma_3 \tag{10}$$

$$\mathbf{n}\cdot\nabla c = 0 \text{ on } \Gamma_{2i} \quad \text{and} \quad \Gamma_{4i}, \quad i = 1\text{–}3 \tag{11}$$

and the initial condition

$$\begin{cases} c = 1 \text{ in } -R_{\text{o}} \leqslant x \leqslant -R_{\text{i}},\ -2.5 \leqslant y \leqslant -1.5 \\ c = 0 \text{ in other regions} \end{cases} \text{ at } t = 0 \tag{12}$$

where the time scale $t_c = L_c/u_c$ and the concentration scale $c_c = c^*_{\text{initial}}$ are used. Here, $R_{\text{o}} = R_{\text{i}} + 1$, the Peclet number ($Pe$) is $u_c L_c/D^*$. In this work, we assume that the fluid speed is about 0.5 mm/s, the channel with is about 100 μm and the diffusivity is $O(10^{-9})$ m^2/s. Then Pe is O(50). The normalized straight channel length is fixed with $L = 5$.

In this work, as a typical value of the Peclet number, we choose $Pe = 50$. The same method can be easily applied to other values of the Peclet number unless it is extremely high. For the cases of extreme values of Peclet number, we need to adopt a different numerical scheme for the solution of the transport equation from the one used here. In the present work, the central difference scheme is used considering accuracy and the not-so-high Peclet number.

2.2. Optimization problem for minimum dispersion

In this work, the optimization problem is to find the zeta potential distributions at the inside and outside walls that minimize the dispersion. We define the optimization problem in which we try to find the zeta potential distributions that minimize the following objective function:

$$\text{Min.} \quad I = \alpha_c \int_\Omega (-c^2)|_{t=t_{\text{f}}}\,\mathrm{d}\Omega + \int_{\Gamma_{\text{cont}}} r^2\,\mathrm{d}\Gamma = \alpha_c I_c + I_{r^2} \tag{13}$$

subject to

$$\nabla\cdot\mathbf{u} = 0 \tag{14}$$

$$\nabla^2\mathbf{u} - \nabla p = 0 \tag{15}$$

$$\frac{\partial c}{\partial t} + \mathbf{u}\cdot\nabla c - \frac{1}{Pe}\nabla^2 c = 0 \tag{16}$$

where α_c is the positive weighting parameter, $\Omega = \Omega_1 \bigcup \Omega_2 \bigcup \Omega_3$ and $\Gamma_{\text{cont}} = \Gamma_{21} \bigcup \Gamma_{22} \bigcup \Gamma_{23} \bigcup \Gamma_{41} \bigcup \Gamma_{42} \bigcup \Gamma_{43}$. Here, r^2 is the norm of velocity difference at the walls defined as

$$r^2 = (u_x - u_x^I)^2 + (u_y - u_y^I)^2 \tag{17}$$

where $\mathbf{u}^I$ is the velocity vector with no control (i.e., $\zeta = 1$ at all walls). At walls, $\mathbf{u}^I = \mathbf{E}$ and $\mathbf{u} = \zeta\mathbf{E}$ and $r^2 = (1-\zeta)^2E^2$ represents some degree of control action for the change of zeta potential.

The first term of the objective function I_c means that maintaining localized high concentration is a better strategy for dispersion control. For more formal treatment, we may use the Schwarz inequality for the inner product and the norms in the function space. If we consider two functions c and 1(unity), then we have

$$|\,\langle c, 1\rangle|^2 \leqslant \|c\|^2\|1\|^2 \tag{18}$$

or

$$\left|\int_\Omega c\,\mathrm{d}\Omega\right|^2 \leqslant \left[\int_\Omega c^2\,\mathrm{d}\Omega\right]\left[\int_\Omega 1\,\mathrm{d}\Omega\right] \tag{19}$$

Since $\int_\Omega 1\,\mathrm{d}\Omega = A =$ area of the domain and $\frac{1}{A}\int_\Omega c\,\mathrm{d}\Omega = \bar{c}$ = average concentration, we have

$$\int_\Omega c^2\,\mathrm{d}\Omega \geqslant A\bar{c}^2 = \text{const.} \tag{20}$$

where the equality holds when $c = \bar{c}$ everywhere in Ω (perfect dispersion case). As we can see above, maintaining localized concentration distribution means that $\int_\Omega c^2 \, d\Omega$ is maximized and the fact justifies the objective function adopted in this work.

Other researchers such as Qiao and Aluru [11] adopted the definition of dispersion based on the product of concentration and the square of the distance from the center of mass. The definition may be efficiently used for the case of considering finite number of particles that are not much dispersed. However, in the present work, that approach has not been adopted in order to avoid the conceptual difficulties arising for the distance between particles across the U-turn.

As mentioned before, the second term of the objective function I_{r^2} is for minimization of the control range. It is a necessary term for solving optimization problem to use the calculus of variations because the variational method needs an objective function which includes one control variable at least. Therefore, the weighting parameter α_c represents the relative importance of minimizing dispersion to the amount of the changed zeta potential. In other words, when α_c is very large, it is a result only to minimize the first term.

The first term of the objective function is changed depending on how t_f is defined. In this work, the final time t_f is defined as the time when the center of mass of analyte arrives at the standard position. The standard position in Ω_3 is defined as the y-axis position that is the same as that for the center of mass of the initial analyte in Ω_1. Therefore, the final time is a function of the concentration distribution controlled by the flow field.

3. Optimality conditions

Adopting the method of the Lagrange multiplier, we introduce the augmented objective function

$$I_a = I + I_p + I_{\mathbf{u}} + I_c \tag{21}$$

Here

$$I_p = \langle \hat{p}, \nabla \cdot \mathbf{u} \rangle \tag{22}$$

$$I_{\mathbf{u}} = \langle \hat{\mathbf{u}}, \nabla^2 \mathbf{u} - \nabla p \rangle \tag{23}$$

$$I_c = \left\langle \hat{c}, \frac{\partial c}{\partial t} + \mathbf{u} \cdot \nabla c - \frac{1}{Pe} \nabla^2 c \right\rangle_t \tag{24}$$

where $\hat{p}$, $\hat{\mathbf{u}}$ and $\hat{c}$ are the Lagrange multipliers which are introduced as the adjoint variables corresponding to the state variables of p, $\mathbf{u}$ and c, respectively. The inner products are defined as

$$\langle \mathbf{A}, \mathbf{B} \rangle = \int_\Omega \mathbf{A} \cdot \mathbf{B} \, d\Omega \tag{25}$$

$$\langle a, b \rangle = \int_\Omega ab \, d\Omega \tag{26}$$

$$\langle a, b \rangle_t = \int_t \int_\Omega ab \, d\Omega \, dt \tag{27}$$

From the optimality condition $\delta I_a = 0$, the Euler–Lagrange equations and the appropriate natural boundary conditions are derived. The basic procedure of deriving the adjoint equations and the natural boundary conditions is introduced in [29]. The expression of δI_a is

$$\delta I_a = \delta I + \delta I_p + \delta I_{\mathbf{u}} + \delta I_c = 0 \tag{28}$$

where

$$\delta I = 2\alpha_c \int_\Omega (-c \delta c)|_{t=t_f} \, d\Omega + \int_{\Gamma_{\text{cont}}} (\mathbf{u} - \mathbf{u}^I) \cdot \delta \mathbf{u} \, d\Gamma \tag{29}$$

$$\delta I_p = \langle \delta \hat{p}, \nabla \cdot \mathbf{u} \rangle - \langle \delta \mathbf{u}, \nabla \hat{p} \rangle + \int_\Gamma \hat{p} (\delta \mathbf{u} \cdot \mathbf{n}) \, d\Gamma \tag{30}$$

$$\begin{aligned} \delta I_{\mathbf{u}} = {} & \langle \delta \hat{\mathbf{u}}, \nabla^2 \mathbf{u} - \nabla p \rangle + \langle \delta \mathbf{u}, \nabla^2 \hat{\mathbf{u}} \rangle + \langle \delta p, \nabla \cdot \hat{\mathbf{u}} \rangle \\ & + \int_\Gamma \mathbf{n} \cdot [(\nabla \delta \mathbf{u}) \cdot \hat{\mathbf{u}} - \nabla \hat{\mathbf{u}} \cdot \delta \mathbf{u} - \mathbf{u} \delta p] \, d\Gamma \end{aligned} \tag{31}$$

$$\begin{aligned} \delta I_c = {} & \left\langle \delta \hat{c}, \frac{\partial c}{\partial t} + \mathbf{u} \cdot \nabla c - \frac{1}{Pe} \nabla^2 c \right\rangle_t \\ & - \left\langle \delta c, \frac{\partial \hat{c}}{\partial t} + \mathbf{u} \cdot \nabla \hat{c} + \frac{1}{Pe} \nabla^2 \hat{c} \right\rangle_t + \langle \delta \mathbf{u}, \hat{c} \nabla c \rangle_t \\ & + \int_\Omega [(\hat{c} \delta c)|_{t=t_f} - (\hat{c} \delta c)|_{t=0}] \, d\Omega \\ & + \int_t \int_\Gamma \mathbf{n} \cdot \left[\left(\frac{\nabla \hat{c}}{Pe} + \mathbf{u} \hat{c} \right) \delta c - \frac{\hat{c}}{Pe} \nabla (\delta c) \right] d\Gamma \, dt. \end{aligned} \tag{32}$$

In order to make $\delta I_a = 0$ for all possible variations of the adjoint variables $\hat{p}, \hat{\mathbf{u}}$ and $\hat{c}$ in the domain, we recover the state equations

$$\nabla \cdot \mathbf{u} = 0 \tag{33}$$

$$\nabla^2 \mathbf{u} - \nabla p = 0 \tag{34}$$

$$\frac{\partial c}{\partial t} + \mathbf{u} \cdot \nabla c - \frac{1}{Pe} \nabla^2 c = 0 \tag{35}$$

On the other hand, from the terms of the variations of the state variables $p, \mathbf{u}$ and c in the domain, the governing equations for the adjoint variables (adjoint equations) are derived as

$$\nabla \cdot \hat{\mathbf{u}} = 0 \tag{36}$$

$$\nabla^2 \hat{\mathbf{u}} - \nabla \hat{p} + \int_t \hat{c} \nabla c \, dt = 0 \tag{37}$$

$$\frac{\partial \hat{c}}{\partial t} + \mathbf{u} \cdot \nabla \hat{c} + \frac{1}{Pe} \nabla^2 \hat{c} = 0 \tag{38}$$

The unspecified boundary conditions of the slip velocity and the boundary conditions of the adjoint variables are derived as the natural boundary conditions from $\delta I_a = 0$. The unspecified boundary conditions of the slip velocity on the wall at which the zeta potential is controlled (Γ_{cont}) is

$$\mathbf{u} \cdot \mathbf{t} = \frac{1}{2} \mathbf{n} \cdot \nabla (\hat{\mathbf{u}} \cdot \mathbf{t}) + \mathbf{u}^I \cdot \mathbf{t} \text{ on } \Gamma_{\text{cont}} \tag{39}$$

Therefore, the boundary conditions for state variables are summarized as

$$\mathbf{u}\cdot\mathbf{n}=-1,\quad \mathbf{u}\cdot\mathbf{t}=0 \text{ on } \Gamma_1 \tag{40}$$

$$\mathbf{u}\cdot\mathbf{n}=0,\mathbf{u}\cdot\mathbf{t} = \frac{1}{2}\mathbf{n}\cdot\nabla(\hat{\mathbf{u}}\cdot\mathbf{t})+\mathbf{u}^{I}\cdot\mathbf{t} \text{ on } \Gamma_{2i} \text{ and } \Gamma_{4i},\quad i=1\text{–}3 \tag{41}$$

$$\mathbf{n}\cdot\nabla(\mathbf{u}\cdot\mathbf{n})=0,\quad \mathbf{u}\cdot\mathbf{t}=0 \text{ on } \Gamma_3 \tag{42}$$

$$c=0 \text{ on } \Gamma_1,\quad \mathbf{n}\cdot\nabla c=0 \text{ on } \Gamma_3 \tag{43}$$

$$\mathbf{n}\cdot\nabla c=0 \text{ on } \Gamma_{2i} \text{ and } \Gamma_{4i},\quad i=1\text{–}3 \tag{44}$$

$$\begin{cases} c=1 \text{ in } -R_o\leqslant x\leqslant -R_i,\ -2.5\leqslant y\leqslant -1.5 \\ c=0 \text{ in other regions} \end{cases} \text{at } t=0 \tag{45}$$

Here, the control variables ζ_{cont} are determined from (41) because the slip velocities at the walls are defined as $\mathbf{u}\cdot\mathbf{t}=\zeta_{cont}(\mathbf{E}\cdot\mathbf{t})=\zeta_{cont}(\mathbf{u}^{I}\cdot\mathbf{t})$. The boundary conditions for the adjoint variables are

$$\hat{\mathbf{u}}\cdot\mathbf{n}=0,\quad \hat{\mathbf{u}}\cdot\mathbf{t}=0 \text{ on all boundaries} \tag{46}$$

$$\hat{c}=0 \text{ on } \Gamma_1,\quad \mathbf{n}\cdot\nabla\hat{c}=-Pe(\mathbf{u}\cdot\mathbf{n})\hat{c} \text{ on } \Gamma_3 \tag{47}$$

$$\mathbf{n}\cdot\nabla\hat{c}=0 \text{ on } \Gamma_{2i} \text{ and } \Gamma_{4i},\quad i=1\text{–}3 \tag{48}$$

$$\hat{c}=2\alpha_c c \text{ at } t=t_f \tag{49}$$

From the mathematical view point, the equation of the adjoint concentration (38) looks like an ill-posed problem. However, (38) is a well-posed problem with the backward time step, because the boundary condition of time is defined at the final time as (49). Even if the equations of (33)–(38) are well defined, the whole system of equations is not easy to solve. Because the equations are highly coupled PDEs, we introduce an iterative method with the relaxation parameter. Since there are no boundary conditions for the pressure p and the adjoint pressure $\hat{p}$, for convenience, we adopt the streamfunction-vorticity method for solving the equations of the flow and the adjoint flow fields. The detailed explanation will be given in Section 4.

4. Numerical implementation

4.1. Streamfunction-vorticity method for the flow and the adjoint flow fields

For the equations of (33,34) and (36,37), there are no boundary conditions of p and $\hat{p}$. Therefore, we use the streamfunction-vorticity formulation method [30] which eliminates the pressure variable in the Navier–Stokes equation. Since this method is well described for the flow field, we simply describe the procedure of the streamfunction-vorticity method for the flow field and the adjoint flow field. Applying the curl operator $(\nabla\times)$ to (34) and (37), the equations of the vorticity $\mathbf{w}$ and the adjoint vorticity $\hat{\mathbf{w}}$ are obtained as

$$\nabla^2\mathbf{w}=0 \tag{50}$$

$$\nabla^2\hat{\mathbf{w}}+\int_t \nabla\hat{c}\times\nabla c\,dt=0 \tag{51}$$

where

$$\mathbf{w}=\nabla\times\mathbf{u} \tag{52}$$

$$\hat{\mathbf{w}}=\nabla\times\hat{\mathbf{u}} \tag{53}$$

In the 2D problem, $\mathbf{w}=(0,0,w_3)=(0,0,w)$ and $\hat{\mathbf{w}}=(0,0,\hat{w}_3)=(0,0,\hat{w})$. The relationships of the streamfunction with the flow and the adjoint streamfunction with the adjoint flow are defined as

$$u_x=-\frac{\partial\psi}{\partial y},\quad u_y=\frac{\partial\psi}{\partial x} \tag{54}$$

$$\hat{u}_x=-\frac{\partial\hat{\psi}}{\partial y},\quad \hat{u}_y=\frac{\partial\hat{\psi}}{\partial x} \tag{55}$$

Since the definitions of (54) and (55), the flow field and the adjoint flow field automatically satisfy the continuity equations of the flow and the adjoint flow, (33) and (36). Substituting (54) and (55) into (52) and (53), the equations of the streamfunction and the adjoint streamfunction are derived as

$$\nabla^2\psi=w \tag{56}$$

$$\nabla^2\hat{\psi}=\hat{w} \tag{57}$$

From (40)–(42) and (46), the boundary conditions for ψ and $\hat{\psi}$ are derived as

$$\psi=x+(1+R_i),\quad \hat{\psi}=0 \text{ on } \Gamma_1 \tag{58}$$

$$\psi=1,\quad \hat{\psi}=0 \text{ on } \Gamma_{2i},\quad i=1\text{–}3 \tag{59}$$

$$\mathbf{n}\cdot\nabla\psi=0,\quad \hat{\psi}=0 \text{ on } \Gamma_3 \tag{60}$$

$$\psi=0,\quad \hat{\psi}=0 \text{ on } \Gamma_{4i},\quad i=1\text{–}3. \tag{61}$$

The boundary conditions for w and $\hat{w}$ are given by (52) and (53). In other words, using ψ, $\hat{\psi}$ and the Dirichlet boundary conditions of $\mathbf{u}$ and $\hat{\mathbf{u}}$, we calculate the values of the Dirichlet boundaries for w and $\hat{w}$ except the boundary condition of w at Γ_3,

$$\mathbf{n}\cdot\nabla w=0 \text{ on } \Gamma_3. \tag{62}$$

By solving the equations of (50) and (56), instead of the continuity equation and the Stokes equation, we can obtain the solution of the flow field without need of the boundary conditions of the pressure. The adjoint flow field is also determined by the equations of (51) and (57).

4.2. Solution procedure

In order to solve the optimality system of Eqs. (50),(51), (56), (57), (35) and (38), we use the finite-difference method (FDM). Considering the value of the Peclet number, we adopted the central difference scheme for the spacewise derivatives. Since the equations are highly coupled, we use the iterative scheme with the relaxation parameter $(\epsilon<1)$. The algebraic system of each variable is solved by the alternating directional implicit (ADI) scheme. The solution procedure is summarized in Fig. 2. The detailed solution procedure is as follows:

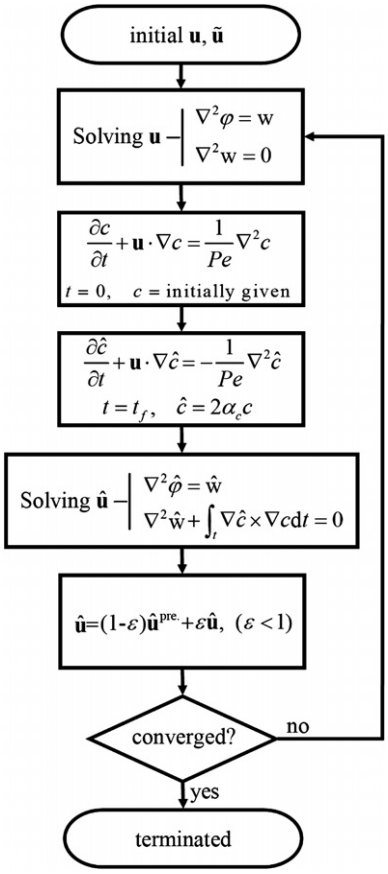

Fig. 2. Flow chart of the solution procedure.

Step 1: Set $\mathbf{u}^{(0)}$, $\hat{\mathbf{u}}^{(0)}$, i=1.
Step 2: Calculate $\mathbf{u}^{(i)}$ from (Step 2-1–2-5).
Step 2-1: Set $\mathbf{w}^{(0)} = \nabla \times \mathbf{u}^{(i-1)}$, j=1.
Step 2-2: Solve (56) for $\psi^{(j)}$ using $\mathbf{w}^{(j-1)}$.
Step 2-3: Calculate $\mathbf{u}^{(j)}$ from (54) using $\psi^{(j)}$.
Step 2-4: Solve (50) for $\mathbf{w}^{(j)}$ with the boundaries defined by $\mathbf{u}^{(j)}$.
Step 2-5: Check convergence.
If not converged, go back to *Step 2-2* and $j = j + 1$.
If converged, $\mathbf{u}^{(i)} = \mathbf{u}^{(j)}$.
Step 3: Calculate and save c at each time step from 0.
Step 3-1: When the analyte arrives at the standard position, t_f is determined and go to *Step 4*.
Step 4: Calculate $\hat{c}$ backwardly at each time step from t_f to 0.
Step 4-1: Read c at each time step and evaluate $\int_t \nabla\hat{c} \times \nabla c\,dt$.
Step 5: Calculate $\hat{\mathbf{u}}^{(i)}$ from *(Step 5-1–5-5)*.
Step 5-1: Set $\hat{\mathbf{w}}^{(0)} = \nabla \times \hat{\mathbf{u}}^{(i-1)}$, j=1.
Step 5-2: Solve (57) for $\psi^{(j)}$ using $\mathbf{w}^{(j-1)}$.
Step 5-3: Calculate $\hat{\mathbf{u}}^{(j)}$ from (55) using $\hat{\psi}^{(j)}$.
Step 5-4: Solve (51) for $\hat{\mathbf{w}}^{(j)}$ with the boundaries defined by $\hat{\mathbf{u}}^{(j)}$.
Step 5-5: Check convergence.
If not converged, go back to *Step 5-2* and $j = j + 1$.
If converged, $\hat{\mathbf{u}}^{(i)} = \hat{\mathbf{u}}^{(j)}$.
Step 6: Update $\hat{\mathbf{u}}^{(i)} = (1-\epsilon)\hat{\mathbf{u}}^{(i-1)} + \epsilon\hat{\mathbf{u}}^{(i)}$
Step 7: Check convergence.
If not converged, go back to *Step 2* and $i = i + 1$.

As discussed in Section 4.1, the flow field and the adjoint flow field are calculated from (50) and (51) and (56) and (57). After the final time and the concentration distribution at the final time are determined in *Step 3*, the adjoint concentration can be solved backwardly from t_f. The numerical value of the integration for $\int_t \nabla\hat{c} \times \nabla c\,dt$ are calculated from the final time to the initial time, because the adjoint concentration is evaluated from t_f to 0. Therefore, we must save the whole information of the concentration at the all time steps. The amount of the saving information is quite large. However, that information is only used in each *i*th iteration and removed. Therefore, the required storage space of saving the massive information is fixed. There are artificial diffusions of the concentration and the adjoint concentration because of using the ADI scheme for the algebraic system of the PDEs discretized by FDM. The solutions of the concentration and the adjoint concentration are influenced by the much stronger diffusion then the diffusion defined by diffusivity. Therefore, the optimal solutions in the work do not accurately include the effect of the diffusion defined by the number of diffusivity. In the procedure, the value of the relaxation parameter is important. In fact, the iterative method without the relaxation parameter (i.e. $\epsilon = 1$) works well when the weighting parameter α_c is small. However, in the optimal problem cases with large α_c, the iterative method without the relaxation parameter shows the fluctuated tendency of error. Due to the fluctuation of error, we introduce the relaxation parameter. The detailed discussion about the relaxation parameter and the convergence of error will be given in the Section 5.

5. Results and discussion

5.1. Preliminary results

Fig. 3 shows the optimal solutions of the the velocity vectors and the concentration distributions at the final time t_f for $\alpha_c = 700$ when $R_i = 1$ and $Pe = 50$. The state variables ($\mathbf{u}$ and $c|_{t=t_f}$) are represented in Fig. 3a. The adjoint variables ($\hat{\mathbf{u}}$ and $\hat{c}|_{t=0}$) are in Fig. 3b. In Fig. 3, the contour plots of the concentration at $t = t_f$ (a) and the adjoint concentration at $t = 0$ (b) are shown. As we can see in Fig. 3a, the optimal zeta potential control results in a successful concentration distribution at $t = t_f$. The detailed analysis of the results for various α_c values will be given later. The distribution of $\hat{c}$ at $t = 0$ in Fig. 3b can also be explained. As mentioned before, the adjoint concentration equation (38) should be solved backwardly. If we define the backward time is $\hat{t} = t_f - t$, then the (38) and (49) are changed to

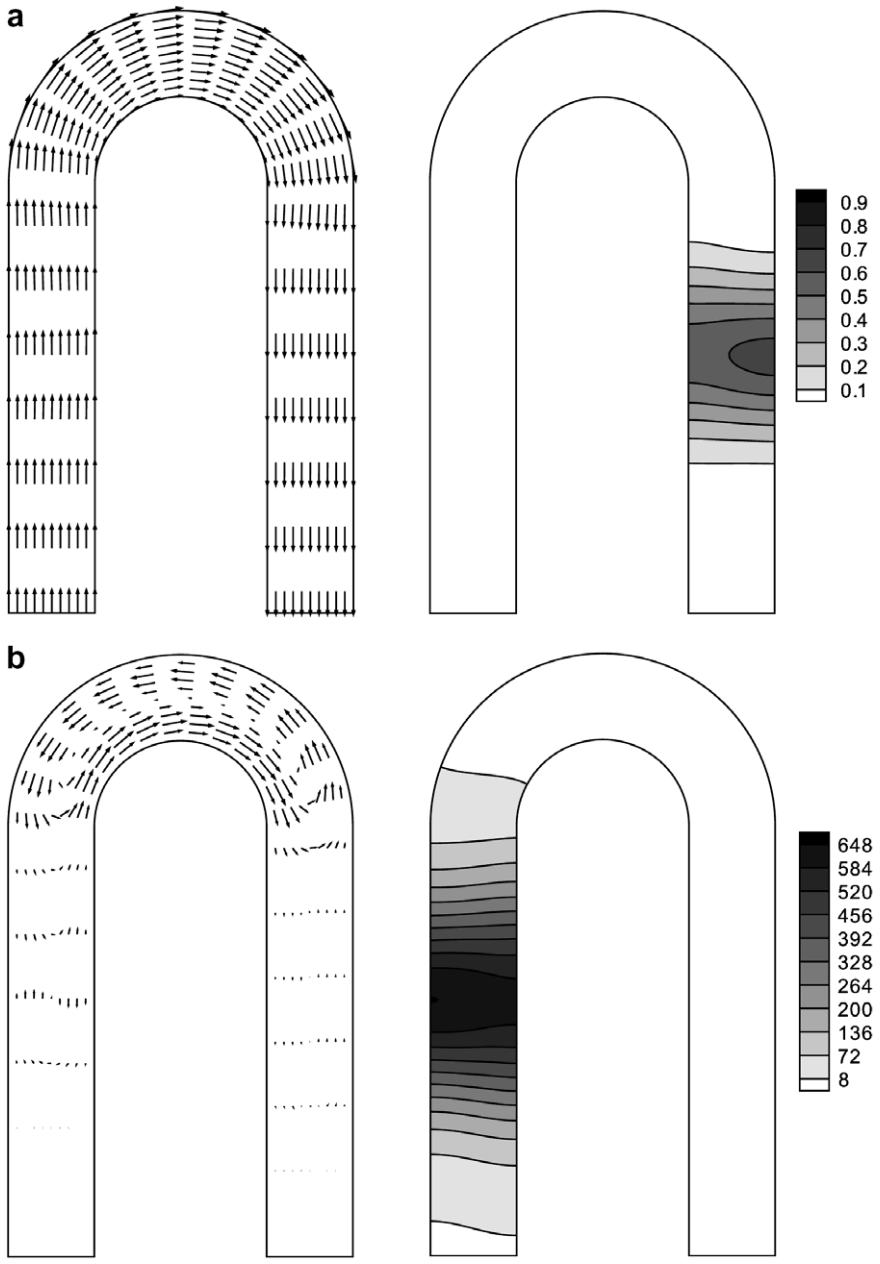

Fig. 3. Vector and contour plots of the optimal solution when $\alpha_c = 700$ with $R_i = 1$ and $Pe = 50$: (a) the flow field and the concentration distribution at the final time and (b) the adjoint flow field and the adjoint concentration distribution at the initial time.

$$\frac{\partial \hat{c}}{\partial \hat{t}} + (-\mathbf{u}) \cdot \nabla \hat{c} = \frac{1}{Pe} \nabla^2 \hat{c} \tag{63}$$

with

$$\hat{c} = 2\alpha_c c|_{t_f} \text{ at } \hat{t} = 0. \tag{64}$$

As we can see above, the governing equation of $\hat{c}$ in terms of the backward time $\hat{t}$ is a convective transport equation with the advection by $(-\mathbf{u})$ and diffusion. Therefore compared with the figure of $c|_{t_f}$ in Fig. 3a ($\hat{c}(\hat{t} = 0) = \hat{c}(t = t_f) = 2\alpha_c c(t = t_f)$), we can see that $\hat{c}(\hat{t} = t_f) = \hat{c}(t = 0)$ is advected backwardly by $(-\mathbf{u})$ and it has wider distribution by diffusion.

5.1.1. Effect of the relaxation parameter

The iterative method with the relaxation parameter works well for various α_c as shown in Fig. 4. Here, the errors are defined as the maximum value of the absolute differences of the velocity norm between the values at the present iteration step and those at the previous step. However, the relaxation parameter should be well chosen to obtain the optimal solution effectively. In this work, the relaxation parameters are determined by

$$\alpha_c \epsilon = \kappa \tag{65}$$

where κ is a constant. At first, κ is a priori determined as $\kappa = 6$ when $\alpha_c = 12$ with $R_i = 1$ and $Pe = 50$. For other

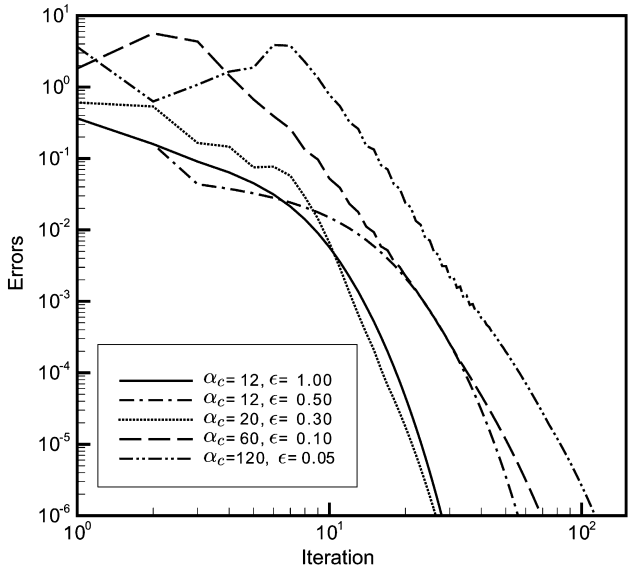

Fig. 4. Numerical errors vs. iteration number for various α_c when $R_i = 1$ and $Pe = 50$.

α_c cases, the relaxation parameters are determined from (65) with $\kappa = 6$. We checked the validity of (65) until $\alpha_c = 700$ and observed that it worked well.

5.1.2. Validation of optimal solution

Let us check if the optimization works properly before discussing the details of the optimal solutions. For validation of the optimal solution, the two kinds of the view points are used. One is to use the calculated values of I_c and I_{r^2} of the objective function (Eq. (13)) for various α_c. The other is comparison between the optimal solution from this work and the result from the work on optimization of localized step-wise zeta potentials [12].

For the given α_c, the objective function is determined by I_c and I_{r^2} in Eq. (13). For various α_c, the values of I_c, I_{r^2} are listed in Table 1. As shown in Table 1, the measure of dispersion I_c decreases and the control range I_{r^2} increases as α_c increases. The dispersion induced by a turn is more suppressed and the variation of the zeta potential distribution from the no control state becomes larger.

Now, for each α_c, we consider the following artificial objective function

$$I'(\alpha_c) = \alpha'_c I_c(\alpha_c) + I_{r^2}(\alpha_c) \tag{66}$$

Table 1
The values of I_c, I_{r^2} of Eq. (13) for the optimal solution with α_c when $R_i = 1$ and $Pe = 50$

	I_c	I_{r^2}
$\alpha_c = 1$	-2.0087×10^{-1}	1.4215×10^{-3}
$\alpha_c = 2$	-2.0424×10^{-1}	5.9210×10^{-3}
$\alpha_c = 3$	-2.0781×10^{-1}	1.3995×10^{-2}
$\alpha_c = 500$	-4.2623×10^{-1}	3.7924
$\alpha_c = 600$	-4.2627×10^{-1}	3.8170
$\alpha_c = 700$	-4.2630×10^{-1}	3.8353

where α'_c is a weighting parameter and $I_c(\alpha_c)$ and $I_{r^2}(\alpha_c)$ are the values evaluated by using the optimal solution for the weighting function α_c. Therefore, $I'(\alpha_c)$ is the value of the objective function for the weighting parameter α'_c when the objective function is evaluated by using the zeta potential distributions that are optimal for the weighting parameter α_c. In each row of Table 2, for a fixed α'_c, the values of objective function are listed for various α_c. As we can see the artificial objective function attains minimum when $\alpha_c = \alpha'_c$. If the column index α_c is not the same as the row index $\alpha'_c (\alpha_c \neq \alpha'_c)$, $I_c(\alpha_c)$ and $I_{r^2}(\alpha_c)$ are not the values evaluated with the optimal solution for the given α'_c. Therefore, the artificial objective function value cannot be smaller than the objective function for the $\alpha_c = \alpha'_c$ case. The optimization method of the present work does not show any contradictory result as can be seen in Table 2, for both the cases with the small variations of $\alpha'_c = 1, 2, 3$ and the cases with the optimal solutions which are asymptotically converged ($\alpha'_c = 500, 600, 700$). In other words, the numerical scheme has passed a necessary test.

Second method for validation is to compare the optimal solution with the known result. According to Woo [12], the optimal flow patterns are well predictable when the inner radius of a turn R_i is very large. When R_i is large, the velocity of the predicted flow for minimum dispersion is proportional to the radius of the position and can be written by

$$\mathbf{u}^{\text{pre}} \cdot \mathbf{t} = \frac{2r}{2R_i + 1}, \mathbf{u}^{\text{pre}} \cdot \mathbf{n} = 0 \text{ in } \Omega_2 \tag{67}$$

where r is the radius of the position. In this work, the predicted zeta potential distributions at the inside and the outside walls are evaluated from the Helmholtz–Smoluchowski speed described in (7) with the known electric field. Thus, the predicted zeta potential distributions at the inside and outside walls are given by

$$\zeta_{\text{in}}^{\text{pre}} = \frac{\mathbf{u}_{\text{in}}^{\text{pre}} \cdot \mathbf{t}}{\mathbf{E} \cdot \mathbf{t}} \text{ on } \Gamma_2 \tag{68}$$

$$\zeta_{\text{out}}^{\text{pre}} = \frac{\mathbf{u}_{\text{out}}^{\text{pre}} \cdot \mathbf{t}}{\mathbf{E} \cdot \mathbf{t}} \text{ on } \Gamma_4 \tag{69}$$

where $\mathbf{u}_{\text{in}}^{\text{pre}} \cdot \mathbf{t} = 2R_i/(2R_i + 1)$ and $\mathbf{u}_{\text{out}}^{\text{pre}} \cdot \mathbf{t} = 2(R_i + 1)/(2R_i + 1)$.

In Fig. 5, the optimal zeta potential distributions at the inside and outsize walls with $\alpha_c = 700, 1000$ and the predicted zeta potential distributions are shown when $R_i = 3$ and $Pe = 50$. For convenience, to represent the zeta potential distributions at the inside and outside walls on the same x-axis, the values are projected on the U-shaped line with fixed radius $R_i = 1$. And the x-axis represents the distance along the center position on the U-shaped line. Therefore, the region of distances from $-\pi/2$ to $\pi/2$ is Ω_2. In Ω_2, the optimal zeta potential distributions obtained from this work agree well with the predicted zeta potential distributions as shown in Fig. 5.

Compared with the model prediction, the optimal solutions have a different tendency of zeta potential distributions in the region between about -3.0 and -4.6. Actually that

Table 2
The values of I' for α_c' ($I'(\alpha_c) = \alpha_c' I_c(\alpha_c) + I_{r^2}(\alpha_c)$) when $R_i = 1$ and $Pe = 50$

	$I'(1)$	$I'(2)$	$I'(3)$	$I'(500)$	$I'(600)$	$I'(700)$
$\alpha_c' = 1$	**−0.1994**	−0.1983	−0.1938	3.3662	3.3907	3.4090
$\alpha_c' = 2$	−0.4003	**−0.4026**	−0.4016	2.9399	2.9644	2.9827
$\alpha_c' = 3$	−0.6012	−0.6068	**−0.6094**	2.5137	2.5382	2.5564
$\alpha_c' = 500$	−100.4343	−102.1126	−103.8934	**−209.3228**	−209.3201	−209.3153
$\alpha_c' = 600$	−120.5214	−122.5363	−124.6749	−251.9459	**−251.9475**	−251.9455
$\alpha_c' = 700$	−140.6086	−142.9600	−145.4564	−294.5689	−294.5749	**−294.5756**

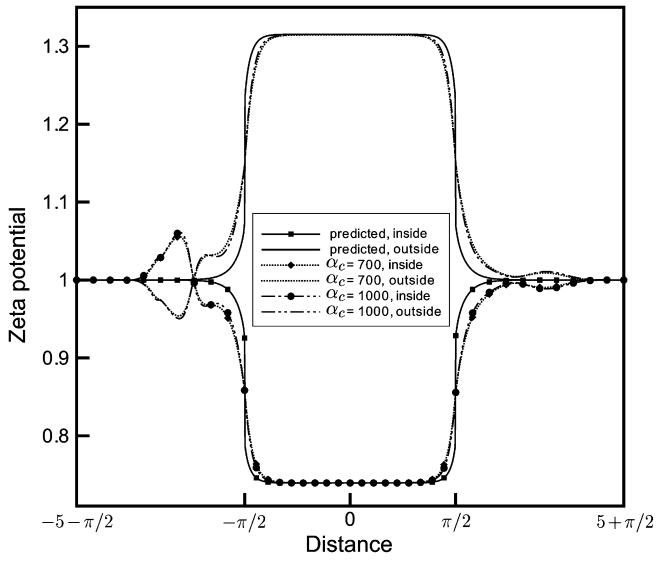

Fig. 5. Comparison the zeta potential distributions of the optimal solutions for $\alpha_c = 700, 1000$ with those of the model prediction when $R_i = 3$ and $Pe = 50$.

region is almost the same with the initially specified non-zero concentration region (from $-\pi/2 - 2.5$ to $-\pi/2 - 1.5$ on x-axis of Fig. 5). The bump in the numerically obtained optimal zeta potential distributions in that region is strongly related with the initial concentration distribution. As shown Fig. 6, the initial concentration distribution is changed by the optimal zeta potential distributions in that region. The rectangular shape of the concentration distribution is changed to the trapezoid shape (like Fig. 6b). This trapezoid-shaped distribution causes less dispersion when the analyte is transported through the curved region (Ω_2) because the optimal flow is slow near the inside wall.

5.2. Effect of the weighting parameter (α_c)

In Fig. 7, the optimal zeta potential distributions at the inside and outside walls for various α_c are shown when $R_i = 1$ and $Pe = 50$. The optimal zeta potential distributions at the inside wall are denoted by the lines with symbols and the optimal zeta potential distributions at the outside wall are denoted by the lines without symbols. When α_c gets larger, the value of the inside zeta potential in Ω_2 becomes smaller and the value of outside zeta potential in Ω_2 becomes larger. The optimal zeta potential distributions

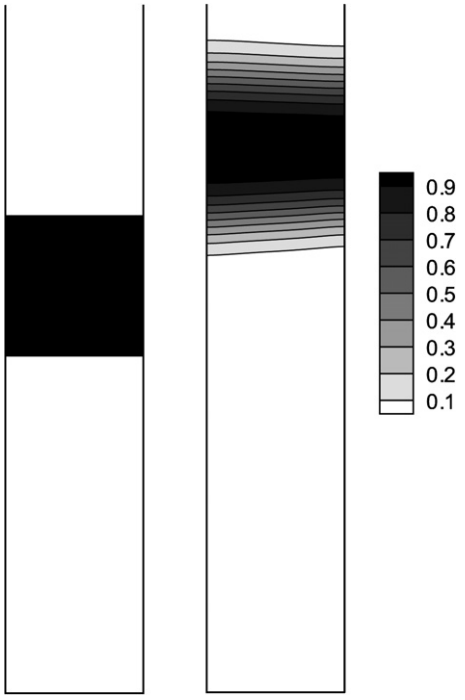

Fig. 6. The contour plots in Ω_1 of concentration for the optimal solution when $\alpha_c = 1000$ with $R_i = 3$ and $Pe = 50$: (a) at $t = 0$ and (b) at $t = 1$.

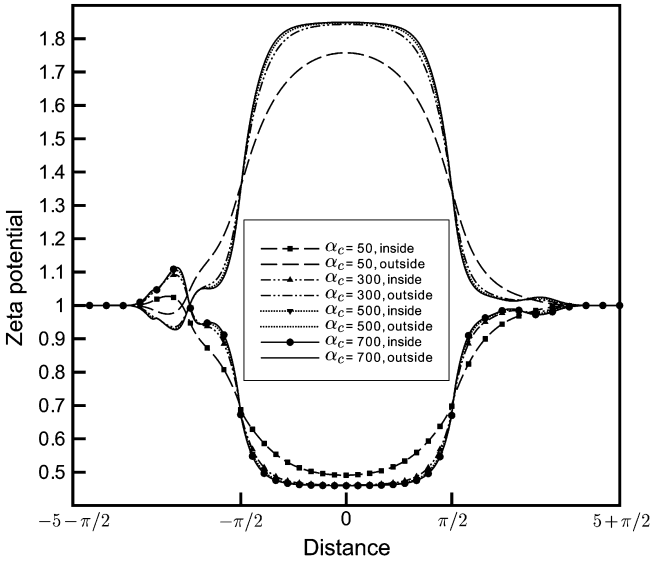

Fig. 7. The effect of the weighting parameter (α_c) on the optimal zeta potential distributions at the inside and outside walls when $R_i = 1$ and $Pe = 50$.

at the inside and outside walls have a tendency of converging to the asymptotic distributions when α_c is extremely large. Therefore, we can estimate the optimal zeta potential distributions without considering the range of the zeta potential from Fig. 7.

As shown in Fig. 8, the dispersion is drastically reduced by the control of the zeta potential distributions at the walls when $R_i = 1$ and $Pe = 50$. For the case of no control, Fig. 8a shows the velocity vector and the concentration distribution at the initial and final times. In Fig. 8b, the velocity vector and the concentration distribution for $\alpha_c = 700$ are shown. For large α_c, the dispersion is dramatically reduced. In Fig. 8, the reason for the tendency of the optimal zeta potential distributions at the walls can be found. In Fig. 8a of the no control case ($\alpha_c = 0$), the race track effect is caused by the faster velocity near the inside wall than near the outside wall. However, the race track effect is reduced by the decreased velocity near the inside wall of a turn and the increased velocity near the outside wall. In Fig. 8b for $\alpha_c = 700$, we can see that the race track effect is minimized by the properly increased zeta potential at the outside wall in Ω_2 and the properly decreased zeta potential at the inside wall in Ω_2.

As previously mentioned, the final time of the objective function is to be determined during the optimization procedure. As shown in Table 3, the final time decreases as α_c

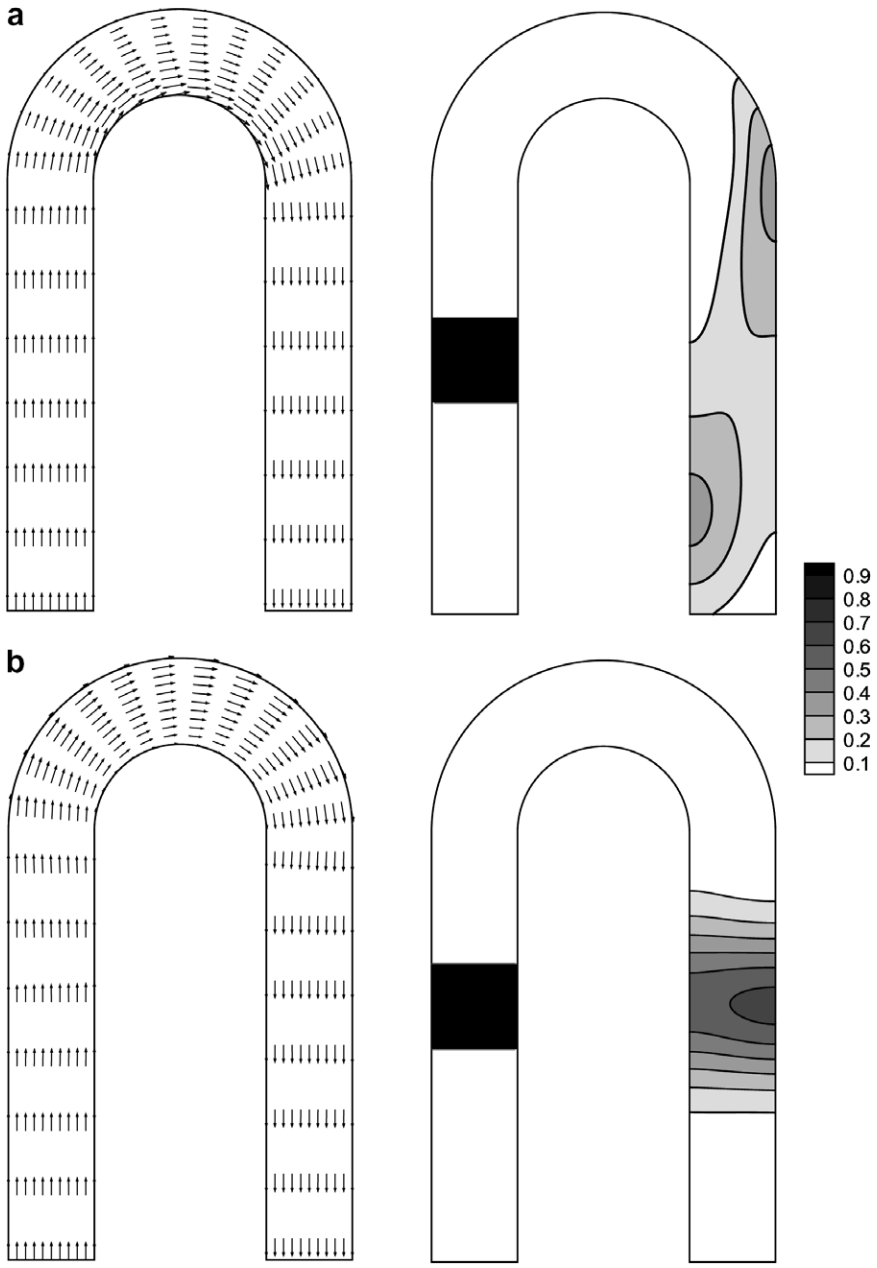

Fig. 8. Velocity vector plots and the contour plots of concentration at $t = t_f$ (with box-shaped initial distribution in Ω_1) when $R_i = 1$ and $Pe = 50$: (a) $\alpha_c = 0$ (no control) and (b) $\alpha_c = 700$.

Table 3
The final time for α_c when $R_i = 1$ and $Pe = 50$

	$\alpha_c = 0$	$\alpha_c = 10$	$\alpha_c = 20$	$\alpha_c = 50$	$\alpha_c = 100$	$\alpha_c = 700$
Final time (t_f)	9.000	8.822	8.754	8.751	8.751	8.751

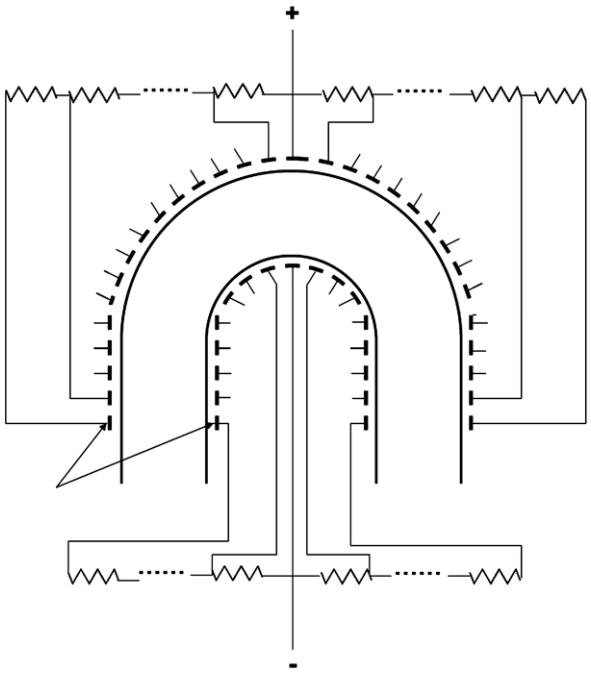

Fig. 9. Schematic of the microchannel system with continuously controlled zeta potential by the external voltage.

increases. However, the final time is not changed after $\alpha_c > 20$. This means that, even if the zeta potential distributions change, the average velocity does not change. As α_c increases, the dispersion is reduced but the position of center of mass does not change anymore.

The optimal solutions obtained in this work are expected to provide valuable information of the optimal control for minimal dispersion and an insight for the design of zeta potential control systems. In addition, the methodology of this work may find further applications for the design of the microchannel system, in which the flow field is to be controlled for various purposes as in the micro-total-analysis-systems (μTAS). One possible example is the mixing problem in an microchannel and some results for the problem are available in [12].

The control system proposed in this work may be fabricated as shown in Fig. 9. Different voltages are supplied to each external electrode to change the zeta potential values at the walls continuously. Application of the electric potential to the external electrode was proved to control the zeta potential value by several previous researchers [9,10,31–33]. In addition, other zeta potential control methods – for example, the patterned surface charge modification [34] and the laser modification of the microchannel surface [35] – are also applicable.

6. Conclusions

A novel type problem is considered for the optimal boundary control with the state equations of the steady flow equations and the unsteady transport equation. Specifically, optimization of the zeta potential distributions at the walls is performed for minimal dispersion in an electroosmotic microchannel. Using the variational approach, we solve the optimal problem. Based on the calculus of variations and the method of Lagrange multiplier, the Euler–Lagrange equations are derived in the form of coupled PDEs. In order to solve the flow equations and the adjoint flow equations, the streamfunction-vorticity method is used to solve the equations without need of the pressure boundary conditions. The iterative method with relaxation parameter is also adopted for stable convergence.

When the optimal zeta potential distributions at both walls are used, the dispersion is marvelously diminished. It is the result of the dramatically reduced race track effect in Ω_2 by the rearranged flow pattern, which is controlled by the optimal zeta potential distributions at the walls. The optimal zeta potential distributions without considering the control range can also be estimated. The optimal zeta potential distributions at the walls have a tendency of converging to the asymptotic distributions when α_c is extremely large. The results of the optimal solutions are expected to provide an insight for the design of zeta potential control systems.

Acknowledgements

This research has been supported by the BK21 program of the Ministry of Education of Korea, by the Grant R01-2004-000-10838-0 from KOSEF and by Center for Ultramicrochemical Process Systems (CUPS) sponsored by KOSEF.

References

[1] E. Zubritsky, Taming turns in micro-channels, Anal. Chem. 72 (2000) 687A.
[2] C.T. Culbertson, S.C. Jacobson, J.M. Ramsey, Dispersion sources for compact geometries on microchips, Anal. Chem. 70 (1998) 3781, doi:10.1021/ac9804487.
[3] C.T. Culbertson, S.C. Jacobson, J.M. Ramsey, Microchip devices for high-efficiency separations, Anal. Chem. 72 (2000) 5814, doi:10.1021/ac0006268.
[4] B.M. Paegel, L.D. Hutt, P.C. Simpson, R.A. Mathies, Turn geometry for minimizing band broadening in microfabricated capillary electrophoresis channels, Anal. Chem. 72 (2000) 3030, doi:10.1021/ac000054r.
[5] S.K. Griffiths, R.H. Nilson, Band spreading in two-dimensional microchannel turns for electrokinetic species transport, Anal. Chem. 72 (2000) 5473, doi:10.1021/ac000595g.
[6] S.K. Griffiths, R.H. Nilson, Design and analysis of folded channels for chip-based separations, Anal. Chem. 74 (2002) 2960, doi:10.1021/ac011218m.
[7] S.K. Griffiths, R.H. Nilson, Low-dispersion turns and junctions for microchannel systems, Anal. Chem. 73 (2001) 272, doi:10.1021/ac000936q.

[8] J.I. Molho, A.E. Herr, B.P. Mosier, J.G. Santiago, T.W. Kenny, R.A. Brennen, G.B. Gordon, B. Mohammadi, Optimization of turn geometries for microchip electrophoresis, Anal. Chem. 73 (2001) 1350, doi:10.1021/ac001127+.

[9] C.-Y. Lee, C.-H. Lin, L.-M. Fu, Band spreading control in electrophoresis microchips by localized zeta-potential variation using field-effect, Analyst 129 (2004) 931, doi:10.1039/b407627n.

[10] G.-B. Lee, L.-M. Fu, C.-H. Lin, C.-Y. Lee, R.-J. Yang, Dispersion control in microfluidic chips by localized zeta potential variation using the field effect, Electrophoresis 25 (2004) 1879, doi:10.1002/elps.200305880.

[11] R. Qiao, N.R. Aluru, Dispersion control in nano-channel systems by localized ζ-potential variations, Sensors Actuat. A 104 (2003) 268, doi:10.1016/d0924-424(03)00029-3.

[12] H.S. Woo, Ph.D. Dissertation, Pohang University of Science and Technology, Korea, 2006.

[13] J.L. Lions, in: S.K. Mitter (Ed.), Optimal Control of Systems Governed by Partial Differential Equations, Springer-Verlag, Berlin, 1971.

[14] R. Glowinski, J.L. Lions, Exact and approximate controllability for distributed parameter systems, Acta Numer. (1994).

[15] M. Gunzburger, Adjoint equation-based methods for control problems in incompressible viscous flows, Flow Turbul. Combust. 65 (2000) 249, doi:10.1023/A:1011455900396.

[16] O. Ghattas, J.-H. Bark, Optimal control of two- and three-dimensional incompressible Navier–Stokes flows, J. Comput. Phys. 136 (1997) 231, doi:10.1006/jcph.1997.5744.

[17] M. Berggren, Numerical solution of a flow-control problem: vorticity reduction by dynamic boundary action, SIAM J. Sci. Comput. 19 (1998) 829, doi:10.1137/S1064827595294678.

[18] M.D. Gunzburger, S. Manservisi, Analysis and approximation of the velocity tracking problem for Navier–Stokes flows with distributed control, SIAM J. Numer. Anal. 37 (2000) 1481, doi:10.1137/S0036142997329414.

[19] J.-W. He, R. Glowinski, R. Metcalfe, A. Nordlander, J. Periaux, Active control, active control and drag optimization for flow past a circular cylinder: I. Oscillatory cylinder rotation, J. Comput. Phys. 163 (2000) 83, doi:10.1006/jcph.2000.6556.

[20] C. Homescu, I.M. Navon, Z. Li, Suppression of vortex shedding for flow around a circular cylinder using optimal control, Int. J. Numer. Methods Fluids 38 (2002) 43, doi:10.1002/fld.203.

[21] H.M. Park, W.J. Lee, J.S. Chung, Boundary optimal control of the Navier–Stokes equations – a numerical approach, Int. J. Eng. Sci. 40 (2002) 2119, doi:10.1016/S0020-72202)00136-2.

[22] M. Hintermüller, K. Kunisch, Y. Spasov, S. Volkwein, Dynamical systems-based optimal control of incompressible fluids, Int. J. Numer. Methods Fluids 46 (2004) 345, doi:10.1002/fld.725.

[23] M. Hinze, K. Kuisch, Second order methods for boundary control of the instationary Navier–Stokes system, Z. Angew. Math. Mech. 84 (2004) 171, doi:10.1002/zamm.200310094.

[24] L.S. Hou, S.S. Ravindran, Computations of boundary optimal control problems for an electrically conducting fluid, J. Comput. Phys. 128 (1996) 319, doi:10.1006/jcph.1996.0213.

[25] G.V. Alekseev, Solvability of control problems for stationary equations of magnetohydrodynamics of a viscous fluid, Siberian Math. J. 45 (2004) 197.

[26] R. Sampath, N. Zabaras, A functional optimization approach to an inverse magneto-convection problem, Comput. Methods Appl. Mech. Eng. 190 (2001) 2063, doi:10.1016/S0045-782(00)00222-X.

[27] S.S. Collis, K. Ghayour, M. Heinkenschloss, M. Ulbrich, S. Ulbrich, Optimal control of unsteady compressible viscous flows, Int. J. Numer. Mech. Fluids 40 (2002) 1401, doi:10.1002/fld.420.

[28] D.R. Reyes, D. Iossifidis, R.-A. Auroux, A. Manz, Micro total analysis systems. 1. Introduction, theory, and technology, Anal. Chem. 74 (2002) 2623, doi:10.1021/ac0202435.

[29] J.H. Jeong, I.S. Kang, Optimization of the crystal surface temperature distribution in the single-crystal growth process by the Czochralski method, J. Comput. Phys. 177 (2002) 284, doi:10.1006/jcph.2002.7011.

[30] L.G. Leal, Laminar Flow and Convective Transport Processes: Scaling Principles and Asymptotic Analysis, Butterworth-Heinemann, Masssachusetts, 1992.

[31] R.B.M. Schasfoort, S. Schlautmann, J. Hendrikse, A. van den Berg, Field-effect flow control for microfabricated fluidic networks, Science 286 (1999) 942, doi:10.1126/science.286.5441.942.

[32] M.A. Hayes, Extension of external voltage control of electroosmosis to high-pH buffers, Anal. Chem. 71 (1999) 3793, doi:10.1021/ac990301v.

[33] C.S. Lee, D. McManigill, C.-T. Wu, B. Patel, Factors affecting direct control of electroosmosis using an external electric field in capillary electrophoresis, Anal. Chem. 63 (1991) 1519, doi:10.1021/ac00015a005.

[34] A.D. Stroock, M. Weck, D.T. Chiu, W.T.S. Huck, P.J.A. Kenis, R.F. Ismagilov, G.M. Whitesides, Patterning electro-osmotic flow with patterned surface charge, Phys. Rev. Lett. 84 (2000) 3314, doi:10.1103/PhysRevLett.84.3314.

[35] T.J. Johnson, D. Ross, M. Gaitan, L.E. Locascio, Laser modification of preformed polymer microchannels: application to reduce band broadening around turns subject to electrokinetic flow, Anal. Chem. 73 (2001) 3656, doi:10.1021/ac010269g.